

Portmanteauing Features for Scene Text Recognition

Yew Lee Tan*, Ernest Yu Kai Chew*
and Adams Wai-Kin Kong
School of Computer Science
and Engineering
Nanyang Technological University (NTU)
Singapore

Jung-Jae Kim
and Joo Hwee Lim
Institute for Infocomm Research
Agency for Science, Technology and Research
Singapore

Abstract—Scene text images have different shapes and are subjected to various distortions, e.g. perspective distortions. To handle these challenges, the state-of-the-art methods rely on a rectification network, which is connected to the text recognition network. They form a linear pipeline which uses text rectification on all input images, even for images that can be recognized without it. Undoubtedly, the rectification network improves the overall text recognition performance. However, in some cases, the rectification network generates unnecessary distortions on images, resulting in incorrect predictions in images that would have otherwise been correct without it. In order to alleviate the unnecessary distortions, the portmanteauing of features is proposed. The portmanteau feature, inspired by the portmanteau word, is a feature containing information from both the original text image and the rectified image. To generate the portmanteau feature, a non-linear input pipeline with a block matrix initialization is presented. In this work, the transformer is chosen as the recognition network due to its utilization of attention and inherent parallelism, which can effectively handle the portmanteau feature. The proposed method is examined on 6 benchmarks and compared with 13 state-of-the-art methods. The experimental results show that the proposed method outperforms the state-of-the-art methods on various of the benchmarks.

I. INTRODUCTION

Scene text recognition (STR) is the task of reading text from natural scenes. The semantic property of text in images embodies additional information that is useful for many practical applications such as intelligent document processing, street signs reading, and product recognition [1]. Because of these important applications, the field has drawn a great amount of attention from researchers and practitioners resulting in the emergence of various robust reading competitions [2]–[6]. STR is challenging because the images are acquired in a generally unstructured and uncontrolled setting. This, in turn, introduces more complexity and variability than traditional optical character recognition (OCR) tasks [1], [7], [8].

An approach in addressing such issues is to employ a rectification network to rectify perspective distorted and curved text before the text recognition process. Yang et al. [9] proposed the use of an auxiliary dense character detection scheme and an alignment loss to improve character localization in order to tackle the issues. In contrast, conceptually simpler methods which do not require explicit character detection are also introduced to address the problems [10], [11].

* these authors contributed equally to this work

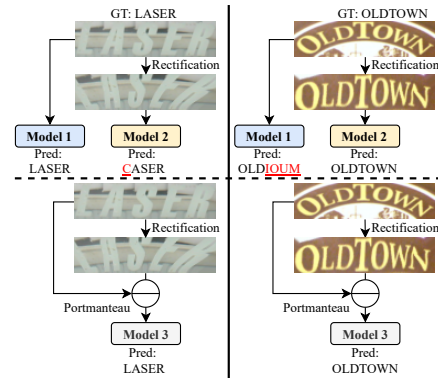


Fig. 1. The prediction results for multiple models from the experiments conducted. Model 1 uses the original image as input while model 2 utilizes a rectification module which rectifies the image before the recognition task. Model 3 uses both the rectified image as well as the original image as the inputs.

Undoubtedly, the usage of rectification network has improved the overall performance of STR. However, the recognition network which comes after the rectification network may experience some form of penalty if, for example, suboptimal rectifications were being performed on regular text images. In other words, the recognition network will suffer from errors propagated from the rectification network, due to its linear input pipeline. An example is illustrated in Figure 1 where the rectification of “LASER” resulted in the loss of information and eventuated an incorrect prediction of “CASER” by model 2.

To mitigate the potential problems that may arise from using the rectification network, this study proposes the *portmanteau feature* which utilizes both the original and rectified images, together with the block matrix initialization, to form a non-linear pipeline. Like a portmanteau word whose meaning is derived from a blending of two or more morphemes (e.g. motel, brunch, smog), the portmanteau feature approach can better preserve the feature of the original image, which lightens the impact of unfavourable rectification, while incorporating the feature of the rectified image. This is shown in Figure 1 where the proposed approach (model 3) is able to generate the correct predictions in both cases as opposed to the model

1 which failed to predict “OLDTOWN” and model 2 which failed to predict “LASER”.

Other than using a rectification network to solve the irregularities of text images, an attention model is also often employed [12], [13] due to its successes in both computer vision and natural language processing [14], [15]. The attention models can be used in tandem with a rectification network as it may be able to encode global context more effectively and hence, improve the overall performance of STR [11], [12], [16], [17].

Although the transformer model (which utilizes attention) [15] was conceptualized for natural language processing (NLP) tasks, it is becoming increasingly popular to be incorporated into vision related tasks due to its capabilities [12], [18], [19]. However, the span of the transformer attention is limited to one axis of direction as NLP tasks mainly involve a sequence of information (or words). As an image contains information in both directions, Dosovitskiy et al. [18] split up the image into patches and arranged them into one sequence as demonstrated in their vision transformer (ViT). However, such method will incur a large amount of computational overhead. Therefore, this work introduces the dual-axes vision transformer (DaViT) which is adapted from the Axial Transformer [20] in order to implicitly attend to features in two axes of direction.

The contribution of this work is as summarized: (1) portmanteau feature containing information from both original and rectified images, lightening the impact of unfavorable rectification, and (2) the proposed network surpasses current state-of-the-art methods.

The rest of the paper is organized as follows. Section II explores related works. Section III discusses the approach and methodology. Section IV reports the experimental results on six scene text benchmarks, and Section V concludes this study.

II. RELATED WORK

Irregular texts present major challenges to STR, and so, Shi et al. and various other works [10], [16], [21], [22] employed geometric transformation using thin plate splines (TPS) with spatial transformer network (STN). Subsequently, promising results from STN spurred several prominent works in text rectification. Luo et al. [11] developed a rectification method, called MORN, free from geometric constraints with the direct prediction of offset maps. Zhan and Lu [22] proposed a STN based rectification network by iteratively rectifying the images, with controls points derived from a polynomial curve and line segments. Yang et al. [23] proposed a rectification module that includes prediction of text center line as well as the various local attributes, all derived from the ground-truth bounding box labels.

Attention mechanism is often utilized in tandem with rectification network in order to enhance the overall performance in STR. Lee and Osindero [24] proposed the use of attention modeling which is conditioned upon the image feature from the CNN as well as the output of the RNN. Wang et al. [25] noticed that various STR works did not make full use

of the alignment history and therefore, proposed the usage of a coverage vector to make adjustment for future attention.

Yu et al. [13] adopted the transformer architecture and introduced a parallel visual attention and a global semantic reasoning module for STR. The network employs a multi-way parallel transmission in order to make use of global semantic information more effectively. Bartz et al. [19] proposed the use of the vanilla transformer in their text recognition network which takes in regions of interest from their localization network.

III. APPROACH

The proposed network can be broken down into three stages as shown in Figure 2. The first stage is the portmanteau feature generation where an input image goes through two different reshaping schemes. One of the schemes reshapes the image into a fixed height with varying width which will be padded to produce a padded image, I_p . The other scheme reshapes the image to a fixed height and fixed width followed by a rectification network to produce a rectified image, I_r . I_r and I_p then form a concatenated image, I_{con} , which goes through a linear projection block and produces the portmanteau feature, F_{port} . The linear projection block utilizes the block matrix initialization which allows the portmanteau feature to retain more individual information from the features of the rectified and padded images.

The second stage is the feature extraction stage that learns representation of the portmanteau feature. A variant of the ViT and Axial Transformer, called the DaViT, is proposed as the basic building block for this stage. By employing the transformer, the network will be able to achieve parallelism in the processing of the portmanteau feature. Furthermore, the DaViT is computationally less intensive than the ViT and Axial Transformer. The feature that transverses through the second stage will also be denoted as F_{port} .

The final stage of the network is the sequence modelling stage which incorporates contextual cues from the sequence of embeddings, as well as the output from the encoder in order to predict the next character. The stage is made up of the vanilla transformer decoder and the softmax function is used to predict the next character.

A. Rectification

Two types of rectification networks are adopted in this study separately, STN and MORN [11]. The TPS of STN makes geometric adjustments to straighten text, while MORN specializes in correcting complex distortion without applying geometric constraints.

In this work, both STN and MORN used are pre-trained. The pre-trained STN follows ASTER STN [10], but instead of predicting the control points directly, it predicts a 4th order Legendre polynomial and 10 line segments to generate the control points, similar to ESIR [22]. Further details regarding the STN are available in the supplementary material. The

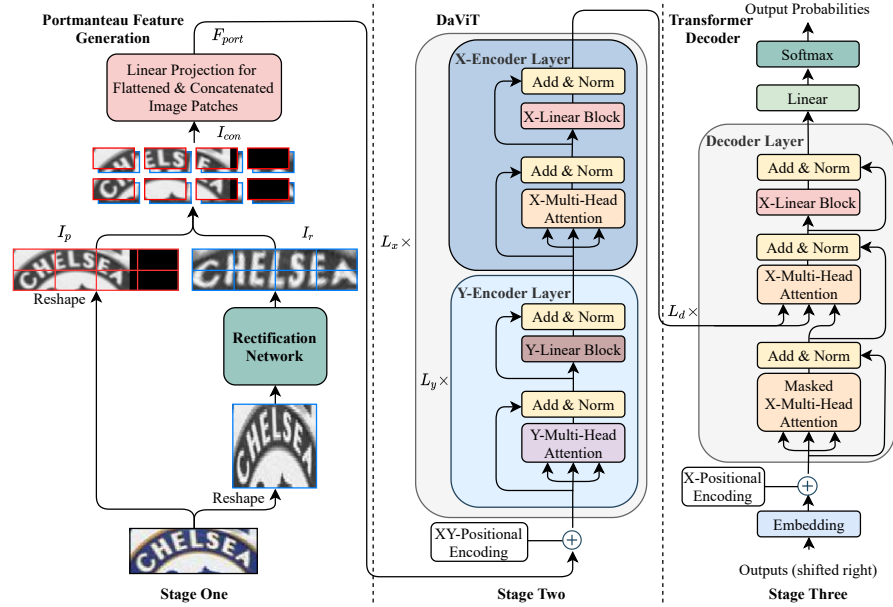


Fig. 2. Overview of the model, illustrating the three stages.

SRNet framework used to train the STN, and the pre-trained MORN are available on GitHub.

B. Portmanteauing Features

A portmanteau word is a blending of two or more words such that the word expresses the combined meaning of its constituents. Like a portmanteau word, a concatenated connection is employed in the first stage of the framework in order to retain the information that exists in the padded image and the rectified image, as illustrated in Figure 2.

1) *Concatenation*: After the reshape and rectification, $I_p \in \mathbb{R}^{H \times W \times 1}$ and $I_r \in \mathbb{R}^{H \times W \times 1}$ are concatenated to form the image $I_{con} = [I_p, I_r]$, where $I_{con} \in \mathbb{R}^{H \times W \times 2}$ and H, W represent the height and width of the image. It is then split up into patches of $P_h \times P_w \times 2$ which is followed by a flattening, resulting in $I_{con} \in \mathbb{R}^{N_x \times N_y \times 2P_w P_h}$, where $N_x = \frac{W}{P_w}$ and $N_y = \frac{H}{P_h}$. I_{con} will then enter a linear projection block (described in Section III-B3), which utilizes the block matrix initialization (described in Section III-B2), and be projected into a portmanteau feature, F_{port} . In the experiments, $P_w = 2$ and $P_h = 4$.

2) *Block Matrix Initialization*: Through the utilization of the transformer's intrinsic property (i.e. the multi-head attention module), the network is able to achieve parallelism in processing the portmanteau feature as if it is going through two separate transformers at the same time.

The block matrix initialization (BMI) scheme is proposed for the parameters in the linear layers in order to regulate the interaction between them. By initializing the parameters as

such, it is assumed that the optimal solution exists within the premise of limited interaction and the network will be able to learn to facilitate the exchange of information with restraint.

The BMI enables I_{con} and F_{port} to start off as though I_{con} is going through two separate linear projection blocks followed by $F_{port} = [F_p, F_r]$ going through two separate transformers. For an arbitrary input $X = [X_1, X_2]$ where $X_1, X_2 \in \mathbb{R}^{N \times D_{in}}$, and $X \in \mathbb{R}^{N \times 2D_{in}}$. The transformation matrix in the linear layer, $A \in \mathbb{R}^{2D_{in} \times 2D_{out}}$, can be broken down into a block matrix as such:

$$A = \begin{bmatrix} A_{11} & A_{12} \\ A_{21} & A_{22} \end{bmatrix}, A_{ij} \in \mathbb{R}^{D_{in} \times D_{out}} \quad (1)$$

By having A_{12} and A_{21} as zero matrices, the linear transformation on X is as though both X_1 and X_2 are going through their individual linear transformation with no interaction between them as follows:

$$XA = [X_1 A_{11} \quad X_2 A_{22}] \quad (2)$$

The two off-diagonal block matrices in each of the linear layers of the encoder are initialized as zero matrices while the diagonal matrices are initialized with the Xavier initialization [26].

3) *Linear Projection*: The linear projection (LP) consists of two linear transformations as shown in Equation 3.

$$LP(I_{con}) = (I_{con} A_1 + b_1) A_2 + b_2 \quad (3)$$

The output of the LP is the portmanteau feature $F_{port} = LP(I_{con})$. For the experiments, the input dimension is $2P_w P_h = 16$, the output dimension D_y which represents the dimensionality of the y-encoder layer is 96, and the inner dimension D_{LP} is 2048.

C. Dual-Axes Vision Transformer Encoder

Scene text images can be densely-packed with characters. Hence, the size of image patches is required to be small enough such that the embedding of every character in the image can be learned. However, the reduction in image patch dimension increases the sequence length. As the complexity of the transformer self-attention layer is $O(N^2D)$ where D is the dimension of the representation, using such a method would be computationally intensive.

In order to solve the above-mentioned issue, an adaptation of the Axial Transformer [20], DaViT encoder is proposed. Instead of an explicit two-dimensional attention of the ViT, Axial Transformer alternates between vertical and horizontal attentions, thereby allowing the model to attend in two axes of direction. The range of patches that the attention can explicitly access will be more limited as compared to ViT in exchange for the reduction in computational overhead. The DaViT further reduces the computational complexity as shown in Table I.

TABLE I
COMPLEXITY OF ViT AND DAViT SELF-ATTENTION LAYER. L_y IS THE NUMBER OF LAYERS FOR THE Y-AXIS ENCODER.

Attention Type	Complexity per Layer
ViT	$O(N_x^2 \cdot N_y^2 \cdot D_x)$
Axial Transformer	$O(N_x^2 \cdot D_x \cdot N_y + N_y^2 \cdot D_x \cdot N_x)$
DaViT	$O(N_x^2 \cdot D_x + N_y \cdot N_x \cdot D_x \cdot L_y)$

The transformer encoder layer that has an attention span across the x-axis is called the x-encoder layer while the one that has its attention span across the y-axis will be called the y-encoder layer as illustrated in the stage two of Figure 2. The y-encoder layer follows its respective architecture in the Axial Transformer where the $N_x = \frac{W}{P_w}$ columns of features will go through the attention mechanism. The feature which transverses through the y-encoder layers with the shape $N_x \times N_y \times D_y$ will have the N_x technically treated as a “mini-batch” size with $N_y = \frac{H}{P_h}$ representing the sequence length.

For the x-encoder layers, F_{port} will be reshaped into $N_x \times D_x$ where the concatenation of D_y through N_y forms D_x ($D_x = D_y \times N_y$) and N_x will represent the sequence length. This is in contrast with the Axial Transformer where the input to corresponding encoder layer would be of the dimension $N_y \times N_x \times D_x$ and the features dimension is the same for both directions ($D_x = D_y$). Specifically for each y-encoder layer, the complexity per layer for DaViT is $N_y^2 \cdot D_y = N_y \cdot N_x \cdot D_x$. Conversely, the counterpart in Axial Transformer has a complexity per layer of $N_y^2 \cdot D_x \cdot N_x$. For the x-encoder layer, the complexity per layer for DaViT is $N_x^2 \cdot D_x$ whereas the complexity for the Axial Transformer is $N_x^2 \cdot D_x \cdot N_y$. In the experiments, the number of x-encoder layers $L_x = 8$, the number of y-encoder layers $L_y = 2$, $N_x = 64$ and $N_y = 8$.

1) *Multi-Head Attention*: Since DaViT performs attention sequentially across both the x and y directions, the model consists of both x and y multi-head attention with each having an attention spanning across the x-axis and y-axis respectively.

According to the transformer [15], the multi-head attention (MHA) is as follows:

$$SDPA(Q, K, V) = softmax\left(\frac{QK^\top}{\sqrt{D/h}}\right)V \quad (4)$$

$$MHA(Q, K, V) = Concat(Att_0, \dots, Att_{h-1})A_M \quad (5)$$

where $Att_i = SDPA(QA_{Q_i}, KA_{K_i}, VA_{V_i})$, i represents the index of the head, and the transformation matrices $A_{Q_i}, A_{K_i}, A_{V_i} \in \mathbb{R}^{D \times \frac{D}{h}}$. For the y-encoder layers, $h_y = 2$ and for the x-encoder layers, $h_x = 16$.

2) *Linear Block*: The linear block (LB) in the network applies two linear layers to each position in the sequence identically, followed by a rectified linear unit (ReLU):

$$LB(F_{port}) = max(0, F_{port}A'_1 + b'_1)A'_2 + b'_2 \quad (6)$$

where $k \in \{x, y\}$, $A'_1 \in \mathbb{R}^{D_k \times D_{LB_k}}$, and $A'_2 \in \mathbb{R}^{D_{LB_k} \times D_k}$. X-linear blocks apply the linear transformations to the sequence along the x-direction whereas the y-linear blocks apply to the y-direction. For the x-linear blocks, the input and output are of the dimension $D_x = 768$, and the inner-layer has the dimensionality of $D_{LB_x} = 2048$. The input and output to the y-linear blocks have the dimensionality of $D_y = 96$ with $D_{LB_y} = 512$.

D. Transformer Decoder

All the building blocks in the decoder are similar to that of DaViT as can be seen on Figure 2. However the masked multi-head attention applies a mask which prevents the attention of subsequent positions (i.e. looking into the future). The decoder is accompanied by a softmax classifier which predicts the probability distribution over the character classes. For the experiments, the number of decoder layers, $L_d = 4$.

IV. EXPERIMENTS

A. Implementation Details

The network was implemented using PyTorch and trained using the ADAM optimizer with a base learning rate of 0.02, betas of (0.9, 0.98), and eps of $1e^{-9}$. The warmup duration was set to 6000 iterations with a decaying rate of $\min(steps^{-0.5}, steps \times warmup^{-1.5})$. The model was trained on 8x NVIDIA RTX6000 24GB, with a batch size of 768 for 300,000 iterations.

The proposed network was trained with three synthetic datasets: *MJSynth* (MJ) [27] containing 9 million samples, *SynthText* (ST) [28] containing 8 million images, and *SynthAdd* (SA) [17] containing 1.6 million images used to compensate for the lack of punctuation in *MJSynth* and *SynthText*.

1) *Scene Text Benchmarks*: The proposed network was evaluated on six scene text benchmarks. *IIIT 5K-Words* (IIIT) [29] contains 3000 test images. *ICDAR 2013* (IC13) [4] contains 1015 images for testing where samples that contain non-alphanumeric characters, or have less than three characters were discarded. *ICDAR 2015* (IC15) [3] contains 2077 test images. *Street View Text* (SVT) [30] consists of 647 testing images. *Street View Text-Perspective* (SVTP) [31] has 645 testing images. *CUTE80* [32] (CT) contains 288 testing images.

TABLE II

TEXT RECOGNITION ACCURACY (IN PERCENTAGES) ON SIX SCENE TEXT BENCHMARKS. FOR EACH BENCHMARK, THE RESULT SHOWN IN **BOLD** REPRESENTS THE BEST PERFORMANCE, WHILE UNDERLINE REPRESENTS THE SECOND BEST. ST, MJ, AND SA DENOTE THE SYNTHETIC DATASETS OF SYNTHTEXT, MJSYNTH, AND SYNTHADD RESPECTIVELY. R DENOTES THE USE OF REAL DATASETS IN TRAINING OR FINE-TUNING. PORT_{MORN} AND PORT_{STN} REPRESENT PORTMANTEAU FEATURE GENERATION USING MORN AND STN, RESPECTIVELY.

Method	Train Datasets	Regular Text			Irregular Text		
		IIIT	IC13	SVT	IC15	SVTP	CT
		3000	1015	647	2077	645	288
Luo et al. [11]	ST+MJ	91.2	92.4	88.3	68.8	76.1	77.4
Yang et al. [23]	ST+MJ	94.4	93.9	88.9	78.7	80.8	87.5
Zhan and Lu [22]	ST+MJ	93.3	91.3	90.2	76.9	79.6	83.3
Wang et al. [33]	ST+MJ	94.3	93.9	89.2	74.5	80.0	84.4
Yu et al. [13]	ST+MJ	94.8	<u>95.5</u>	91.5	-	85.1	87.8
Zhang et al. [34]	ST+MJ	94.7	94.2	90.9	-	81.7	-
Qiao et al. [35]	ST+MJ	93.8	92.8	89.6	80.0	81.4	83.6
Bartz et al. [19]	ST+MJ+SA	94.6	93.1	89.2	74.2	83.1	89.6
Port _{STN} +DaViT	ST+MJ	93.8	95.0	94.3	<u>80.3</u>	89.9	<u>88.5</u>
Port _{MORN} +DaViT	ST+MJ+SA	95.3	96.0	91.0	79.9	<u>87.8</u>	83.3
Port _{STN} +DaViT	ST+MJ+SA	<u>95.1</u>	94.3	<u>92.3</u>	80.5	87.6	86.8
Yue et al. [36]	ST+MJ+R	<u>95.4</u>	<u>94.1</u>	89.3	<u>79.2</u>	82.9	92.4
Wan et al. [37]	ST+MJ+R	95.7	94.9	<u>92.7</u>	-	<u>84.8</u>	<u>91.6</u>
Port _{STN} +DaViT	ST+MJ+R	95.0	<u>94.1</u>	94.1	82.5	90.0	87.8
Li et al. [17]	ST+MJ+SA+R	<u>95.0</u>	94.0	91.2	78.8	86.4	89.6
Lu et al. [12]	ST+MJ+SA+R	<u>95.0</u>	95.3	90.6	<u>79.6</u>	84.5	87.5
Hu et al. [16]	ST+MJ+SA+R	95.8	<u>94.4</u>	<u>92.9</u>	79.5	85.7	92.2
Port _{STN} +DaViT	ST+MJ+SA+R	<u>95.0</u>	<u>93.6</u>	94.6	82.7	87.0	89.2

TABLE III

RESULT OF ABLATION STUDY FOR PORTMANTEAU FEATURE, IN TERMS OF TEXT RECOGNITION ACCURACY (IN PERCENTAGES). THE '(U)' IN THE METHOD NAMES REPRESENTS RESIZING THE IMAGES WITHOUT PADDING.

Method	Regular Text			Irregular Text			Avg. Acc
	IIIT	IC13	SVT	IC15	SVTP	CT	
	3000	1015	647	2077	645	288	
Port _{STN} +DaViT	95.1	94.3	92.3	80.5	87.6	86.8	89.9
Port _{STN} +DaViT (U)	94.8	95.5	93.7	75.7	88.2	89.6	88.9
Port _{STN} +DaViT w/o BMI	94.9	94.9	92.3	80.2	87.3	87.2	89.8
Port _{STN} +DaViT w/o BMI (U)	94.7	96.4	93.5	75.8	87.4	88.5	88.7
STN+DaViT	95.1	93.9	92.1	79.6	87.9	86.8	89.6
DaViT	94.3	95.7	90.9	77.0	83.4	84.7	88.2

B. Experimental Results

The network recognizes 100 token classes, including 10 digits, 52 case sensitive letters, 35 punctuation characters, a start token, an end token, and a pad token. During evaluation, only 37 classes which include 36 case-insensitive alphanumeric characters and an end token were taken into consideration. The maximum output sequence length is 30 and greedy decoding was used. No rotation strategy [17] was used in the experiments.

The network was evaluated on six benchmarks and the comparison results are given in Table II. The results show that the proposed network with MORN (Port_{MORN}+DaViT) outperforms the original MORAN [11] significantly for all the test datasets. Moreover, both Port_{MORN}+DaViT and Port_{STN}+DaViT which utilize a full Transformer encoder-decoder architecture outperforms KISS [19] and MASTER [12], where both networks are ResNet-Transformer hybrids.

The result demonstrates the benefit of the transformer encoder over the ResNet.

Furthermore, the proposed models achieved state-of-the-art result for the majority of the datasets with Port_{STN}+DaViT leading IC15 (containing 2077 images) by 0.9% and SVTP (containing 645 images) by 1.2%. Comparing the results of other works which included real datasets in the training or fine-tuning process, Port_{STN}+DaViT achieved 82.7% accuracy on IC15 and 94.6% on SVT, outperforming the next best results from other works by 2.7% and 1.7% respectively. Although there is a drop in the accuracy for SVTP when real datasets are included, the result of 87.0% still outperforms the next best result from otherworks by 0.6%.

C. Ablation Studies

1) *Discussion on Portmanteauing Feature*: Two additional networks were trained without the portmanteau feature in order to investigate its impact as follows: (1) the STN+DaViT which

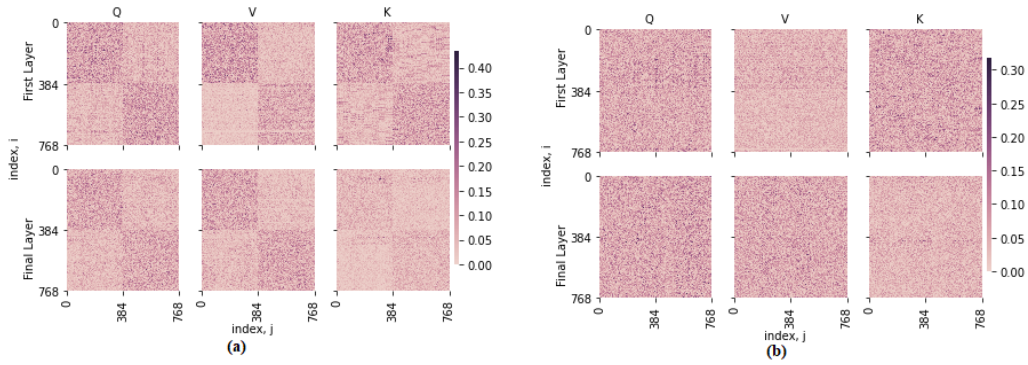


Fig. 3. Heat maps of the Q, V, K linear layers parameters for the x-multi-head attention in the first and last encoder layers for (a) with BMI and (b) without BMI. The absolute values of the parameters are shown to illustrate with a better contrast.

contains a rectification network, and (2) the DaViT with only I_p as the input. The two networks were trained with the same hyperparameters as Port_{STN}+DaViT.

Table III shows the result of the experiments. To a certain extent, it demonstrates that the introduction of the STN causes an adverse impact to the text recognition capability of the model. Such effect is explicitly evident on the IC13 dataset as the accuracy dropped by 1.8% when STN is added into DaViT although the average accuracy on the datasets increases. Figure 4 shows some examples from the test datasets on the adverse effect of the STN on the predictions and the alleviation of the effect by portmanteauing of features. More examples are provided in the supplementary material.

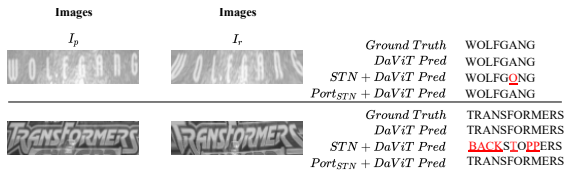


Fig. 4. Examples from the test datasets on the adverse effect of STN on the predictions.

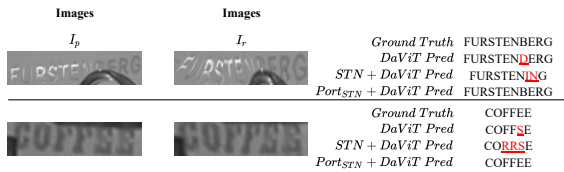


Fig. 5. Examples from the test datasets.

Comparing Port_{STN}+DaViT with STN+DaViT and DaViT, where only one image was used, shows that the portmanteauing of feature generally improves the overall accuracy of the test datasets. The network, appears to be able to mitigate the adverse effect of STN as it outperforms STN+DaViT on four benchmarks including IC13 dataset. The incorporation of

the features from I_p and I_r also allows the network to attain higher accuracy on SVT and IC15 than what could have been achieved individually. Some examples are shown in Figure 5 where the Port_{STN}+DaViT is able to attain correct predictions for the text images where both DaViT and STN+DaViT result in wrong predictions. More examples are provided in the supplementary material.

From Table III, it appears that BMI slightly improves the average accuracy of the test datasets. It is interesting to note that the parameters of the linear layers in Port_{STN}+DaViT with BMI is able to retain the characteristic of the block matrix initialization after the training as seen on Figure 3. Such patterns can be observed in all linear layers where the block matrix initialization was used. This suggests that a more optimal solution exists where the interaction between the features of the two images are regulated by the BMI.

Furthermore, results from Table III show that using the same reshaping scheme of unpadding for both images (i.e. method names denoted by “U”) results in worst overall performance. Although some datasets benefited from this, there is a drop of about 1% in average accuracy across the 6 benchmarks as compared with their counterparts (without “U”).

V. CONCLUSION

In this paper, the adverse impact of rectification network was discussed. Although the rectification network improves overall text recognition accuracy, this study found that in some instances, rectification network can produce undesirable results. In order to address this issue, the portmanteauing of feature was proposed together with DaViT which can effectively handle the portmanteau feature. Experimental results show that the approach, to a certain extent, was able to lighten the adverse impact of rectification and also achieved the state-of-the-art results for most scene text recognition benchmarks.

VI. ACKNOWLEDGEMENT

This work is partially supported by NTU Internal Funding – Accelerating Creativity and Excellence (NTU-ACE2020-03).

REFERENCES

- [1] S. Long, X. He, and C. Yao, "Scene text detection and recognition: The deep learning era," *International Journal of Computer Vision*, vol. 129, no. 1, pp. 161–184, 2021.
- [2] S. M. Lucas, A. Panaretos, L. Sosa, A. Tang, S. Wong, R. Young, K. Ashida, H. Nagai, M. Okamoto, H. Yamamoto *et al.*, "Icdar 2003 robust reading competitions: entries, results, and future directions," *International Journal of Document Analysis and Recognition*, vol. 7, no. 2-3, pp. 105–122, 2005.
- [3] D. Karatzas, L. Gomez-Bigorda, A. Nicolaou, S. Ghosh, A. Bagdanov, M. Iwamura, J. Matas, L. Neumann, V. R. Chandrasekhar, S. Lu *et al.*, "Icdar 2015 competition on robust reading," in *Proceedings of the 13th International Conference on Document Analysis and Recognition*, 2015, pp. 1156–1160.
- [4] D. Karatzas, F. Shafait, S. Uchida, M. Iwamura, L. G. i Bigorda, S. R. Mestre, J. Mas, D. F. Mota, J. A. Almazan, and L. P. De Las Heras, "Icdar 2013 robust reading competition," in *Proceedings of the International Conference on Document Analysis and Recognition*, 2013, pp. 1484–1493.
- [5] R. Gomez, B. Shi, L. Gomez, L. Numann, A. Veit, J. Matas, S. Belongie, and D. Karatzas, "Icdar 2017 robust reading challenge on coco-text," in *Proceedings of the IAPR International Conference on Document Analysis and Recognition*, vol. 1, 2017, pp. 1435–1443.
- [6] C. Rigaud, D. Doucet, Antoine, M. Coustaty, and J.-P. Moreux, "Icdar 2019 competition on post-ocr text correction," in *Proceedings of the International Conference on Document Analysis and Recognition*, 2019, pp. 1588–1593.
- [7] X. Chen, L. Jin, Y. Zhu, C. Luo, and T. Wang, "Text recognition in the wild: A survey," *ACM Computing Surveys*, vol. 54, no. 2, pp. 1–35, 2021.
- [8] Y. Zhu, Y. Cong, and X. Bai, "Scene text detection and recognition: Recent advances and future trends," *Frontiers of Computer Science*, vol. 10, no. 1, pp. 19–36, 2016.
- [9] X. Yang, D. He, Z. Zhou, D. Kifer, and C. L. Giles, "Learning to read irregular text with attention mechanisms," in *Proceedings of the International Joint Conference on Artificial Intelligence*, vol. 1, 2017, p. 3.
- [10] B. Shi, M. Yang, X. Wang, P. Lyu, C. Yao, and X. Bai, "Aster: An attentional scene text recognizer with flexible rectification," *IEEE Transactions on Pattern Analysis and Machine Intelligence*, vol. 41, no. 9, pp. 2035–2048, 2018.
- [11] C. Luo, L. Jin, and Z. Sun, "Moran: A multi-object rectified attention network for scene text recognition," *Pattern Recognition*, vol. 90, pp. 109–118, 2019.
- [12] N. Lu, W. Yu, X. Qi, Y. Chen, P. Gong, and R. Xiao, "Master: Multi-aspect non-local network for scene text recognition," *arXiv preprint arXiv:1910.02562*, 2019.
- [13] D. Yu, X. Li, C. Zhang, T. Liu, J. Han, J. Liu, and E. Ding, "Towards accurate scene text recognition with semantic reasoning networks," in *Proceedings of the IEEE Conference on Computer Vision and Pattern Recognition*, June 2020.
- [14] P. Anderson, X. He, C. Buehler, D. Teney, M. Johnson, S. Gould, and L. Zhang, "Bottom-up and top-down attention for image captioning and visual question answering," in *Proceedings of the IEEE Conference on Computer Vision and Pattern Recognition*, 2018, pp. 6077–6086.
- [15] A. Vaswani, N. Shazeer, N. Parmar, J. Uszkoreit, L. Jones, A. N. Gomez, E. Kaiser, and I. Polosukhin, "Attention is all you need," in *Advances in Neural Information Processing Systems*, vol. 30, 2017.
- [16] W. Hu, X. Cai, J. Hou, S. Yi, and Z. Lin, "Gtc: Guided training of ctc towards efficient and accurate scene text recognition," in *Proceedings of the AAAI Conference on Artificial Intelligence*, vol. 34, 2020, pp. 11 005–11 012.
- [17] H. Li, P. Wang, C. Shen, and G. Zhang, "Show, attend and read: A simple and strong baseline for irregular text recognition," in *Proceedings of the AAAI Conference on Artificial Intelligence*, vol. 33, July 2019, pp. 8610–8617.
- [18] A. Dosovitskiy, L. Beyer, A. Kolesnikov, D. Weissenborn, X. Zhai, T. Mostafa, M. Dehghani, M. Minderer, G. Heigold, S. Gelly, J. Uszkoreit, and N. Houlsby, "An image is worth 16x16 words: Transformers for image recognition at scale," in *Proceedings of the 9th International Conference on Learning Representations*, 2021.
- [19] C. Bartz, J. Bethge, H. Yang, and C. Meinel, "Kiss: Keeping it simple for scene text recognition," *arXiv preprint arXiv:1911.08400*, 2019.
- [20] J. Ho, N. Kalchbrenner, D. Weissenborn, and T. Salimans, "Axial attention in multidimensional transformers," *arXiv preprint arXiv:1912.12180*, 2019.
- [21] B. Shi, X. Bai, and C. Yao, "An end-to-end trainable neural network for image-based sequence recognition and its application to scene text recognition," *IEEE Transactions on Pattern Analysis and Machine Intelligence*, vol. 39, no. 11, pp. 2298–2304, 2016.
- [22] F. Zhan and S. Lu, "Esir: End-to-end scene text recognition via iterative image rectification," in *Proceedings of the IEEE Conference on Computer Vision and Pattern Recognition*, June 2019.
- [23] M. Yang, Y. Guan, M. Liao, X. He, K. Bian, S. Bai, C. Yao, and X. Bai, "Symmetry-constrained rectification network for scene text recognition," in *Proceedings of the IEEE International Conference on Computer Vision*, October 2019.
- [24] C.-Y. Lee and S. Osindero, "Recursive recurrent nets with attention modeling for ocr in the wild," in *Proceedings of the IEEE Conference on Computer Vision and Pattern Recognition*, June 2016.
- [25] C. Wang, F. Yin, and C.-L. Liu, "Memory-augmented attention model for scene text recognition," in *Proceedings of the 16th International Conference on Frontiers in Handwriting Recognition*, 2018, pp. 62–67.
- [26] X. Glorot and Y. Bengio, "Understanding the difficulty of training deep feedforward neural networks," in *Proceedings of the 13th International Conference on Artificial Intelligence and Statistics*, ser. Proceedings of Machine Learning Research, vol. 9, May 2010, pp. 249–256.
- [27] M. Jaderberg, K. Simonyan, A. Vedaldi, and A. Zisserman, "Synthetic data and artificial neural networks for natural scene text recognition," *arXiv preprint arXiv:1406.2227*, 2014.
- [28] A. Gupta, A. Vedaldi, and A. Zisserman, "Synthetic data for text localisation in natural images," in *Proceedings of the IEEE Conference on Computer Vision and Pattern Recognition*, 2016, pp. 2315–2324.
- [29] A. Mishra, K. Alahari, and C. Jawahar, "Scene text recognition using higher order language priors," in *Proceedings of the British Machine Vision Conference*, 2012.
- [30] K. Wang, B. Babenko, and S. Belongie, "End-to-end scene text recognition," in *Proceedings of the International Conference on Computer Vision*, 2011, pp. 1457–1464.
- [31] T. Q. Phan, P. Shivakumara, S. Tian, and C. L. Tan, "Recognizing text with perspective distortion in natural scenes," in *Proceedings of the IEEE International Conference on Computer Vision*, 2013, pp. 569–576.
- [32] A. Risnumawan, P. Shivakumara, C. S. Chan, and C. L. Tan, "A robust arbitrary text detection system for natural scene images," *Expert Systems with Applications*, vol. 41, no. 18, pp. 8027–8048, 2014.
- [33] T. Wang, Y. Zhu, L. Jin, C. Luo, X. Chen, Y. Wu, Q. Wang, and M. Cai, "Decoupled attention network for text recognition," in *Proceedings of the AAAI Conference on Artificial Intelligence*, vol. 34, April 2020, pp. 12 216–12 224.
- [34] H. Zhang, Q. Yao, M. Yang, Y. Xu, and X. Bai, "Autostr: Efficient backbone search for scene text recognition," in *Proceedings of the European Conference on Computer Vision*, 2020, pp. 751–767.
- [35] Z. Qiao, Y. Zhou, D. Yang, Y. Zhou, and W. Wang, "Seed: Semantics enhanced encoder-decoder framework for scene text recognition," in *Proceedings of the IEEE Conference on Computer Vision and Pattern Recognition*, June 2020.
- [36] X. Yue, Z. Kuang, C. Lin, H. Sun, and W. Zhang, "Robustscanner: Dynamically enhancing positional clues for robust text recognition," in *Proceedings of the European Conference on Computer Vision*, Cham, 2020, pp. 135–151.
- [37] Z. Wan, M. He, H. Chen, X. Bai, and C. Yao, "Textscanner: Reading characters in order for robust scene text recognition," in *Proceedings of the AAAI Conference on Artificial Intelligence*, vol. 34, April 2020, pp. 12 120–12 127.

Supplementary Material for: Portmanteauing Features for Scene Text Recognition

Yew Lee Tan, Ernest Yu Kai Chew
and Adams Wai-Kin Kong
School of Computer Science
and Engineering
Nanyang Technological University
Singapore

Jung-Jae Kim
and Joo Hwee Lim
Institute for Infocomm Research
Agency for Science, Technology and Research
Singapore

I. STN

A. Input Protocols for Portmanteau Features

To generate portmanteau features, the raw images were first converted into grayscale images, before being normalized via two transformation protocols.

The first protocol resized the image to a fixed height of 32 pixels with varying width to retain the aspect ratio. After this resizing, if the width of the image was shorter than 128 pixels, zero padding would be applied. Otherwise, the width of the image would be further resized to 128 pixels.

The second protocol directly resized the input image to 300×300 pixels for STN and 32×128 pixels for MORN. The size of the output images from the two rectification networks is 32×128 pixels. Both protocols would yield grayscale images with a size of 32×128 pixels.

The STN was trained with a batch size of 32 for 150 epochs, with a configuration of initial learning rate as $5e^{-4}$, the warm-up iteration was 10,000, and the decay per iteration was set such that the final learning rate is one-fifth of its initial. The Adam optimizer used was configured with betas of (0.9, 0.999), and an eps of $1e^{-8}$. Lastly, the STN dataset contains 80,000 synthetic images with a 9-to-1 train-validation split.

In addition, the STN also adopts a custom loss function, which is defined as:

$$L_{STN} = \|\psi - \hat{\psi}\| + \alpha \|\phi - \hat{\phi}\| + \beta \|\cos \theta - \cos \hat{\theta}\| + \gamma \|\sin \theta - \sin \hat{\theta}\| + \delta \|\xi - \hat{\xi}\| \quad (1)$$

where $\|\bullet\|$ represents L1 norm, $\hat{\psi}$ is the estimated coefficients of the 4th order Legendre polynomial, $\hat{\theta}$ is the estimated angles between the line segments and the tangents of the polynomial, $\hat{\phi}$ is the estimated x-coordinates of the intersection points between the line segments and the polynomial, and $\hat{\xi}$ is the length of the line segments. ψ, θ, ϕ , and ξ are the corresponding ground truths and α, β, γ , and δ are hyperparameters. It should be highlighted that the area between the predicted and ground-truth polynomial is directly proportional to the difference between their Legendre coefficients.

B. Polynomial Scheme for STN

The polynomial scheme could be dividing into six parts, as follows:

- 1) extracting the key points from the ground-truth bounding boxes
- 2) fitting the polynomial curve and lines, using the extracted key points
- 3) determining the intersection points between the polynomial and its line segments
- 4) interpolating the intersection points and the line angles to get the desired number of line segments
- 5) converting the coefficients of the fitted polynomial into its Legendre equivalence
- 6) combining all the variables into a single loss function

Key points extraction: The first step in the polynomial scheme was to resize the image into a square image. The height and width of the square image were considered to be in the range of -1 and 1.

Subsequently, the top-center, center and bottom-center of each bounding box, in addition to the top, center and bottom of the left-most and right-most corners, were extracted as key points for curve and line fitting. These key points were denoted as the green and red points in Figure 1b.

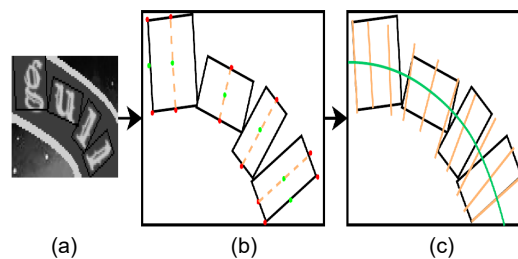


Fig. 1. Overview of the STN polynomial scheme, where the ground-truth bounding boxes were used to derive a 4th order polynomial with 10 line segments.

Curve and line fitting: After which, the center key points were used to fit a 4th order polynomial, while the top, center,

and bottom points were used to fit $(n + 2)$ linear functions, where n was the number of characters in the word.

Intersection between polynomial and line: Then, the intersection points between the polynomial and the $n + 2$ line segments were determined and denoted as ϕ_{raw} . The angles between the tangent lines and the line segments were also calculated and denoted as θ_{raw} . In addition, the height of the tallest bounding box was computed and denoted as ξ .

Line segments interpolation: Next, ϕ_{raw} and θ_{raw} would be used as key reference points for rotational and translational interpolation to produce the desired number of line segments (from $n + 2$) of length ξ . In this paper, the desired number of line segments was set to 10 (See Figure 1c).

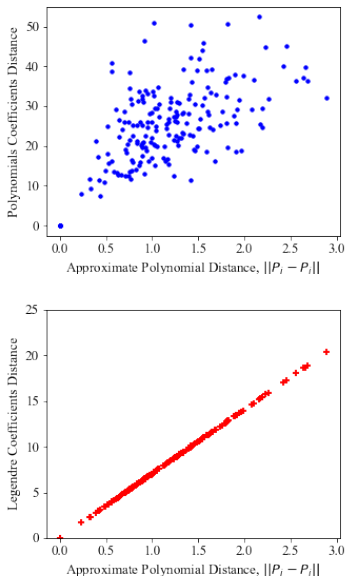


Fig. 2. The scatter plots of polynomial coefficients distance (top) and Legendre coefficients distance (bottom) of 400 polynomial pairs against $\|P_i - P_j\|$.

Legendre polynomial: Then, the coefficients of the polynomial would be converted to its Legendre equivalence. This is because Legendre polynomials form a complete orthogonal basis on $L^2 [-1,1]$ (L^2 space) [?] and so, their coefficients may be better for measuring the similarity between two polynomials.

Figure 2 was constructed with 20 random polynomials $f_i(x)$, where $i \in [1, 20]$. Each polynomial was paired with each other to form 400 polynomial pairs. $N = 201$ evenly distributed points across the x -axis from $[-1, 1]$ were sampled from each polynomial and the y values form a point, P_i , where $P_i \in \mathbb{R}^N$. The 400 polynomial pairs were represented as in the scatter plots, in terms of the distance, $\|P_i - P_j\|$, and the $\|coef(f_i) - coef(f_j)\|$, where $i, j \in [1, 20]$ and $coef(\cdot)$ returns the coefficients of its polynomial function.

Although the polynomial coefficient distances seemly correlate with the distance $\|P_i - P_j\|$ (top of Figure 2), they did

not demonstrate proportionality like its Legendre equivalence (bottom of Figure 2), which was the reason Legendre coefficients were used in this work instead.

Loss function:

$$L_{STN} = \|\psi - \hat{\psi}\| + \alpha \|\phi - \hat{\phi}\| + \beta \|\cos \theta - \cos \hat{\theta}\| + \gamma \|\sin \theta - \sin \hat{\theta}\| + \delta \|\xi - \hat{\xi}\| \quad (2)$$

where $\|\bullet\|$ represents L1 norm, $\hat{\psi}$ is the estimated coefficients of the 4th order Legendre polynomial, $\hat{\theta}$ is the estimated angles between the line segments and the tangents of the polynomial, $\hat{\phi}$ is the estimated x-coordinates of the intersection points between the line segments and the polynomial, and $\hat{\xi}$ is the length of the line segments. ψ, θ, ϕ , and ξ are the corresponding ground truths and α, β, γ , and δ are hyperparameters.

C. STN configurations

Layers	Output Size	Configurations
ConvBlock1	$32 \times 50 \times 50$	$3 \times 3, BN, ReLU, 2 \times 2$
ConvBlock2	$64 \times 25 \times 25$	$3 \times 3, BN, ReLU, 2 \times 2$
ConvBlock3	$32 \times 12 \times 12$	$3 \times 3, BN, ReLU, 2 \times 2$
ConvBlock4	$16 \times 6 \times 6$	$3 \times 3, BN, ReLU, 2 \times 2$
FC1	512	$BN, ReLU$
FC2	$3 \times M + 5$	None

TABLE I

THE CONFIGURATIONS OF STN ARE SHOWN IN THIS TABLE. THE CONFIGURATION VALUES ARE ARRANGED SEQUENTIALLY AS FOLLOWS: KERNEL SIZE, NORMALIZATION LAYER, ACTIVATION LAYER, AND MAX-POOLING. M REFERS TO THE NUMBER OF LINE SEGMENTS, WHICH WAS SET TO 10.

Table I shows the configurations for the localization network within the STN. While the STN takes an input image with a resolution of 300×300 pixels, the localization network requires an image with a resolution of 100×100 pixels. This implementation is faithful to ASTER STN [?], which also uses down-sampled images for control points prediction.

However, unlike ASTER STN, the localization network here does not output the control points directly. Instead, it predicts 5 polynomial coefficients, as well as $\hat{\phi}$, $\hat{\theta}$, and $\hat{\xi}$ for each of the 10 line segments. Therefore, altogether the localization network's output size is 35 for each image, and these 35 values are converted into 30 control points.

D. Discussion on control points

Figure 3 shows that the rectified images using three control points can better mitigate character-level distortions, and many curved characters from before are straightened when the midpoints are introduced. Moreover with the midpoints, the rectified polynomial forms a straight line across the image, which better aligns with the expected rectified outcome. Therefore, in this work, the use of three control points per line segment is favored, in contrast with similar polynomial scheme [?] which uses only the line segments' endpoints.

Do note that control points predicted outside the image are clamped to the image boundary as per the implementation of ASTER STN, and in that case, the truncated line segment may cause some distortions in the rectified image.

Method	Regular Text			Irregular Text			Avg. Acc
	IIIT	IC13	SVT	IC15	SVTP	CT80	
	3000	1015	647	2077	645	288	7672
DaViT	94.3	95.7	90.9	77.0	83.4	84.7	88.2
SaViT	94.3	95.6	90.4	76.5	83.9	81.3	88.0 _(-0.2)
STN+DaViT	95.1	93.9	92.1	79.6	87.9	86.8	89.6
STN+SaViT	94.5	94.0	92.4	78.5	87.4	86.8	89.0 _(-0.6)

TABLE II

RESULT OF ABLATION STUDY FOR DAViT, IN TERMS OF TEXT RECOGNITION ACCURACY (IN PERCENTAGES). THE SUBSCRIPT IN THE CELL REPRESENTS ITS RELATIVE ACCURACY WITH RESPECT TO ITS DUAL-AXES COUNTERPART.

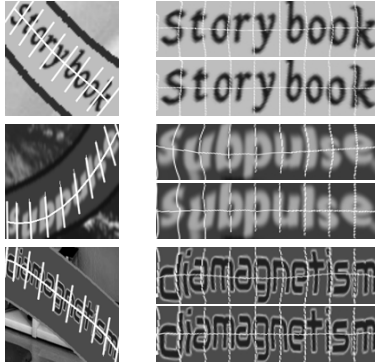


Fig. 3. Rectification results of STN using only the line segment endpoints (top) vs. endpoints + midpoint (bottom).

Table II shows the result of the experiments where DaViT generally enhances the overall performance as compared to SaViT with a significant improvement in the irregular test datasets. This suggests that the attention in both axes allows the network to learn a feature representation that is stronger against distortions.

III. EXAMPLES FROM TEST DATASETS

Figures 5,6,7 show the examples of predictions results from the models.

E. STN training dataset

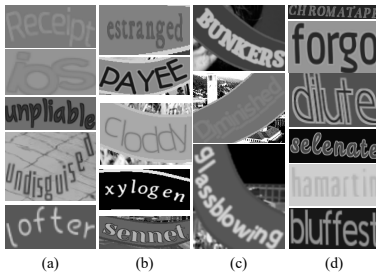


Fig. 4. Examples of the 4 types of training data for the STN: (a) curved texts, (b) curved texts with background stripes, (c) curved texts with background stripes & image rotation, and lastly, (d) simple straight text.

The STN training set containing four types of images shown in Figure 4 was generated by the SRNet framework [?]. Customization were made to add a single band of solid-color stripe as the image background. In this paper, 20,000 samples were generated for each type of training data.

II. DISCUSSION ON DAViT

In order to study the effectiveness of DaViT, the y-encoder layers were removed and the resulting model is denoted as SaViT. For the training of SaViT, the input image was sliced into $N_x \times P_w H$ strips (as opposed to patches of $P_w P_h$), where $P_w = 2$ and $N_x = 64$. The attention for SaViT only spans across the sequence of strips through the x-encoder layers.

		Groundtruth DaViT Prediction STN+DaViT Prediction PortSTN+DaViT Prediction	SPECIAL SPECIM_ SPECINE SPECIAL
		Groundtruth DaViT Prediction STN+DaViT Prediction PortSTN+DaViT Prediction	SKIN SILVIN SHIN SKIN
		Groundtruth DaViT Prediction STN+DaViT Prediction PortSTN+DaViT Prediction	MONTHLY MOANIFY MORRINRY MONTHLY
		Groundtruth DaViT Prediction STN+DaViT Prediction PortSTN+DaViT Prediction	LTD LIU LEW LTD
		Groundtruth DaViT Prediction STN+DaViT Prediction PortSTN+DaViT Prediction	GNC GIF GNP GNC
		Groundtruth DaViT Prediction STN+DaViT Prediction PortSTN+DaViT Prediction	FURSTENBERG FURSTENBERG FURSTENING FURSTENBERG
		Groundtruth DaViT Prediction STN+DaViT Prediction PortSTN+DaViT Prediction	FISH FUN_ ESSN FISH
		Groundtruth DaViT Prediction STN+DaViT Prediction PortSTN+DaViT Prediction	FENDI FERM_ FEND_ FENDI
		Groundtruth DaViT Prediction STN+DaViT Prediction PortSTN+DaViT Prediction	ESPLANADE ESCAPED RESOLVED ESPLANADE
		Groundtruth DaViT Prediction STN+DaViT Prediction PortSTN+DaViT Prediction	COFFEE COFFSE CORRSE COFFEE
		Groundtruth DaViT Prediction STN+DaViT Prediction PortSTN+DaViT Prediction	BACKI BACK_ BACK_ BACKI
		Groundtruth DaViT Prediction STN+DaViT Prediction PortSTN+DaViT Prediction	2015 Q015 15 2015

Fig. 5. Examples showing that the combination of failure cases from both DaViT and STN+DaViT, eventually produces accurate predictions when Port_{STN}+DaViT was applied instead.

Width-Padded Images, I_p	Rectified Images, I_r	Groundtruth	WOLFGANG
		DaViT Prediction	WOLFGANG
		STN+DaViT Prediction	WOLFGONG
		PortSTN+DaViT Prediction	WOLFGANG
		Groundtruth	TRANSFORMERS
		DaViT Prediction	TRANSFORMERS
		STN+DaViT Prediction	BACKSTOPPERS
		PortSTN+DaViT Prediction	TRANSFORMERS
		Groundtruth	RESIDENCE
		DaViT Prediction	RESIDENCE
		STN+DaViT Prediction	RESIDENCES
		PortSTN+DaViT Prediction	RESIDENCE
		Groundtruth	PIZZA
		DaViT Prediction	PIZZA
		STN+DaViT Prediction	PAZZA
		PortSTN+DaViT Prediction	PIZZA
		Groundtruth	NA
		DaViT Prediction	NA
		STN+DaViT Prediction	WA
		PortSTN+DaViT Prediction	NA
		Groundtruth	LION
		DaViT Prediction	LION
		STN+DaViT Prediction	TION
		PortSTN+DaViT Prediction	LION
		Groundtruth	LASER
		DaViT Prediction	LASER
		STN+DaViT Prediction	CASER
		PortSTN+DaViT Prediction	LASER
		Groundtruth	I
		DaViT Prediction	I
		STN+DaViT Prediction	-
		PortSTN+DaViT Prediction	I
		Groundtruth	INTEL
		DaViT Prediction	INTEL
		STN+DaViT Prediction	INFEL
		PortSTN+DaViT Prediction	INTEL
		Groundtruth	G
		DaViT Prediction	G
		STN+DaViT Prediction	OR
		PortSTN+DaViT Prediction	G
		Groundtruth	BETRIEBSBEREIT
		DaViT Prediction	BETRIEBSBEREIT
		STN+DaViT Prediction	RETREIBSBEREIT
		PortSTN+DaViT Prediction	BETRIEBSBEREIT
		Groundtruth	34
		DaViT Prediction	34
		STN+DaViT Prediction	3A
		PortSTN+DaViT Prediction	34

Fig. 6. Examples where correct predictions was achieved by Port_{STN}+DaViT mitigating the adverse impacts of rectification.

Width-Padded Images, I_p	Rectified Images, I_r	Groundtruth	
		Groundtruth DaViT Prediction STN+DaViT Prediction PortSTN+DaViT Prediction	STARBUCKS STAMBUCKS STARBUCKS STARBUCKS
		Groundtruth DaViT Prediction STN+DaViT Prediction PortSTN+DaViT Prediction	COFFEE COFFIE COFFEE COFFEE
		Groundtruth DaViT Prediction STN+DaViT Prediction PortSTN+DaViT Prediction	START STAR_ START START
		Groundtruth DaViT Prediction STN+DaViT Prediction PortSTN+DaViT Prediction	FINISH <u>LINTER</u> FINISH FINISH
		Groundtruth DaViT Prediction STN+DaViT Prediction PortSTN+DaViT Prediction	MICHAEL <u>ANCHOR</u> MICHAEL MICHAEL
		Groundtruth DaViT Prediction STN+DaViT Prediction PortSTN+DaViT Prediction	DENVER <u>SE</u> NVER DENVER DENVER
		Groundtruth DaViT Prediction STN+DaViT Prediction PortSTN+DaViT Prediction	GRANDSTAND <u>COMMITTEEWOMAN</u> GRANDSTAND GRANDSTAND
		Groundtruth DaViT Prediction STN+DaViT Prediction PortSTN+DaViT Prediction	SALMON <u>FROM</u> SALMON SALMON
		Groundtruth DaViT Prediction STN+DaViT Prediction PortSTN+DaViT Prediction	COMPANY <u>AND</u> COMPANY COMPANY
		Groundtruth DaViT Prediction STN+DaViT Prediction PortSTN+DaViT Prediction	ITALIAN <u>T</u> ALIAN ITALIAN ITALIAN
		Groundtruth DaViT Prediction STN+DaViT Prediction PortSTN+DaViT Prediction	WELCOME <u>BILLIONTH</u> WELCOME WELCOME
		Groundtruth DaViT Prediction STN+DaViT Prediction PortSTN+DaViT Prediction	PIONEER <u>LONER</u> PIONEER PIONEER

Fig. 7. Examples showing that portmanteau features did not prevent the model from leveraging the benefits of rectification networks.